Reduction of Torque Ripple in Direct Torque Control for Induction Motor Drives Using Decoupled Amplitude and Angle of Stator Flux Control

Yuttana Kumsuwan[1],

Watcharin Srirattanawichaikul[2], and Suttichai Premrudeepreechacharn[3] Non-members

ABSTRACT

This paper proposes design and implementation of a direct torque controlled induction motor drive system. The method is based on decouple control of the amplitude and the angle of the stator flux reference for determining the reference stator voltage vector in generating the PWM output voltage for induction motors. The objective is to reduce electromagnetic torque ripple and stator flux droop which result in a decrease in current distortion at steady state. The proposed technique is based on the relationship between the instantaneous slip angular frequency and rotor angular frequency in adjustment of the stator flux angle reference. The amplitude of the reference stator flux is always kept constant at rated value. The system has been implemented to verify its capability such as torque and stator flux responses, stator phase current distortion both during dynamic and steady state with load variation, and low speed operation.

1. INTRODUCTION

Direct torque control (DTC) of induction motor drives offers high performance in terms of simplicity in control and fast electromagnetic torque response. Because of its dominant characteristics, the direct torque controlled induction motor drive is becoming popular in industrial applications. The principle of the classical DTC is its decoupled control of stator flux and electromagnetic torque using hysteresis control of the stator flux and torque error and stator flux position. A switching look-up table is included for selection of voltage vectors feeding the induction motor [1]-[3]. However, the main problem is that when operating at steady state, the DTC produces high level of torque ripple, variable switching frequency of inverter over a fundamental period, and stator flux droop during adjacent vector of a voltage vector change. More-

over, particularly when induction motor with DTC operates under heavy load condition in low speed region, distortion of the motor phase current is increased due to stator flux droop leading to reduced drive system efficiency [4]-[8].

Improved performance of DTC for overcoming the drawback of the classical DTC is done by application of voltage modulation replacing look-up table of the voltage vector selection on the basis of 2-level inverter. The voltage modulation is based on space vector modulation (SVM) with constant switching frequency for applying to the induction motor. This technique can be classified into 4 main types according to the control structure as follows. The first method is called DTC-SVM control [9]-[11].This method is based on the deadbeat control derived from the torque and stator flux errors. It offers good steady state and dynamic performance with reduction in phase current distortion, and fast response of torque. However, this technique has limitation in being computationally intensive. The second method is called Adaptive Neural Fuzzy Inference system (ANIS) [12], [13]. This method is based on fuzzy logic and artificial neural network for decoupled stator flux and torque control. Voltage vectors are performed in polar coordinates. Good steady-state and dynamic performance is achieved. The third method is called stator flux oriented control (SFOC): The technique uses two proportional-integral (PI) controllers instead of hysteresis controllers for generating direct and quadrature components from stator flux and torque, respectively. Voltage vectors are performed in Cartesian coordinates. This method provides good transient performance, robustness and reduced steady-state torque ripple [14]-[18]. The last method is called DTC-SVM with closed loop torque control. This method uses only one output of the PI controller. The stator flux positions are estimated and the amplitude of the reference stator flux is kept constant for determining the reference stator flux vector. Then the resultant error between the actual stator flux and the reference stator flux is used for voltage vector calculation. Performance of the control system depends on the design of PI torque controller [19], [20].

In this paper, DTC based on decoupled control

of both stator flux and torque is proposed which is different from DTC-SVM [9]-[20]. This technique uses the relationship between torque, slip angular frequency and rotor angular frequency for controlling stator flux angle while the amplitude of the reference stator flux is kept constant at rated value. Then, the reference stator flux vector in polar form is determined.

This paper is organized as follows. Section II describes dynamic model of induction motor in two-phase stationary reference frame. Section III derives the proposed direct torque control by decoupling the amplitude and angle of the stator flux vector (DTC-AAS). This section also describes the design of PI torque controller, determination of reference voltage vector derived from resultant error between the actual and required stator flux vectors. In addition, the improvement of stator flux estimation is also discussed. Comparative performance results from experimental setup between the proposed method and the classical DTC are given in section IV. Finally, the main features and advantages of the proposed technique are summarized in the conclusions.

2. INDUCTION MOTOR MODEL

The dynamic model of an induction motor in the stationary reference frame can be written in $\alpha\beta$ reference frame variables. Stator voltage vector $\bar{v}_s$ of the motor can be expressed as follows.

$$
\begin{aligned}
v_{\alpha s} &= \frac{d}{dt}\psi_{\alpha s} + R_s i_{\alpha s} \\
v_{\beta s} &= \frac{d}{dt}\psi_{\beta s} + R_s i_{\beta s} \\
\bar{v}_s &= \frac{d}{dt}\bar{\psi}_s + R_s \bar{i}_s.
\end{aligned}
\tag{1}
$$

The stator flux vector $\bar{\psi}_s$ and components can be written as

$$
\begin{aligned}
\psi_{\alpha s} &= L_s i_{\alpha s} + L_m i_{s\alpha} \\
\psi_{\beta s} &= L_s i_{\beta s} + L_m i_{s\beta} \\
\bar{\psi}_s &= L_s \bar{i}_s + L_m \bar{i}_s.
\end{aligned}
\tag{2}
$$

and the rotor flux vector $\bar{\psi}_r$ and components in the stationary reference frame is

$$
\begin{aligned}
\psi_{\alpha r} &= L_r i_{\alpha r} + L_m i_{r\alpha} \\
\psi_{\beta r} &= L_r i_{\beta r} + L_m i_{r\beta} \\
\bar{\psi}_r &= L_r \bar{i}_r + L_m \bar{i}_s.
\end{aligned}
\tag{3}
$$

where $v_{\alpha s}$ and $v_{\beta s}$ are the stator voltages; $i_{\alpha s}$ and $i_{\beta s}$ are the stator currents; $i_{\alpha r}$ and $i_{\beta r}$ are the rotor currents; $\psi_{\alpha s}$ and $\psi_{\beta s}$ are the stator fluxes; $\psi_{\alpha r}$ and $\psi_{\beta r}$ are the rotor fluxes; $\bar{i}_s$ and $\bar{i}_r$ are the stator and rotor current vectors; R_s is the stator winding resistance;

and L_s, L_r, L_m are stator, rotor self inductance and mutual inductance, respectively.

The electromagnetic torque T_e developed by the induction motor in terms of stator and rotor flux vectors can be expressed as

$$
\begin{aligned}
T_e &= \frac{3}{2}P\frac{L_m}{\sigma L_s L_r}\bar{\psi}_s \times \bar{\psi}_r = \frac{3}{2}P\frac{L_m}{\sigma L_s L_r}|\bar{\psi}_s||\bar{\psi}_r|\sin(\rho_s - \rho_r) \\
&= \frac{3}{2}P\frac{L_m}{\sigma L_s L_r}|\bar{\psi}_s||\bar{\psi}_r|\sin(\delta).
\end{aligned}
\tag{4}
$$

where $\sigma = 1 - L_m^2/L_s L_r$ is the leakage factor; P is the number of pole pairs, and δ is the torque angle

From the above equation, clearly, the electromagnetic torque is cross vector product of the stator and rotor flux vectors. Therefore, generally torque control can be performed by controlling torque angle with constant amplitude of the stator and rotor fluxes.

3. PROPOSED CONTROL METHOD

Fig. 1 shows the block diagram of the DTC-AAS drive system. The control system consists of four basic functions, namely the torque control, PI torque controller, the polar-to-rectangular transformation of direct stator flux control and a stator voltage calculation blocks, and the stator flux and torque estimation block. Description of each block is as follows.
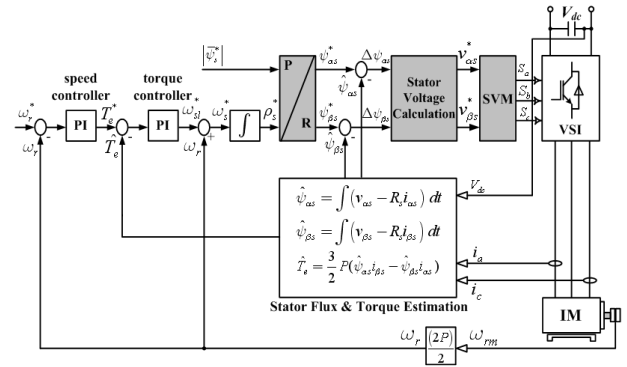

Fig.1: Block diagram of the DTC-AAS drive system

A. Torque Control

In this method, the torque control is performed by defining the constant amplitude of reference stator flux $|\bar{\psi}_s^*|$. When considering (4), rotor flux vector rotates after the stator flux vector with torque angle δ at constant amplitude. Torque control is directly performed by controlling the torque angle δ change which is the angle between stator and rotor flux vectors. According to (2) and (3), with constant amplitudes of both stator and rotor fluxes, stator and rotor flux vectors in terms of stator angular frequency ω_s and rotor angular frequency ω_r and the position of both flux vectors rotating with angle ρ_s and p_r with respect to real axis in the stationary reference frame, respectively, as shown in Fig.2, are written as follows.

$$\bar{\psi}_s(t) = |\bar{\psi}_s^*|e^{j\rho_s} = |\bar{\psi}_s^*|e^{j\omega_s t} \qquad (5)$$

$$\bar{\psi}_r(t) = |\bar{\psi}_r^*|e^{j\rho_r}. \qquad (6)$$
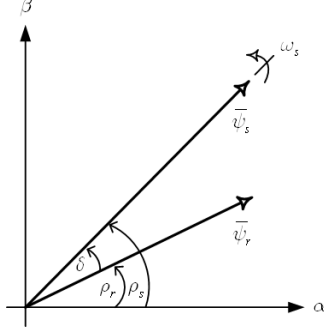
Fig.2: *Stator and rotor flux vectors*

With the same principle in [9], by substituting (5) and (6) into (4), the instantaneous electromagnetic torque can be derived as

$$T_e(t) = \frac{3}{2}P\frac{L_m}{\sigma L_s L_r}|\bar{\psi}_s^*|e^{j\omega_s t} \times \bar{\psi}_r(t)$$
$$= \left[\frac{3}{2}P\frac{L_m^2}{R_r L_s^2}|\bar{\psi}_s^*|^2\right]\left[1 - e^{-\frac{t}{T_M}}\right](\omega_s - \omega_r). \quad (7)$$

where R_r is the rotor winding resistance, and $T_M = \sigma\frac{L_r}{R_r}$ is the time constant.

From (7), the quantity $(\omega_s - \omega_r)$, which is the relationship between stator angular frequency ω_s and rotor speed ω_r, is slip angular frequency ω_{sl} and can be written as

$$\omega_{st} = \omega_s - \omega_r. \qquad (8)$$

The rotor speed ω_r is related to the actual mechanical speed by the pole pairs, therefore the rotor speed is given by,

$$\omega_r = \frac{(2P)}{2}\omega_{rm}. \qquad (9)$$

where ω_{rm} is the mechanical speed

By substituting (8) into (7), the instantaneous electromagnetic torque is given by,

$$T_e(t) = \left[\frac{3}{2}P\frac{L_m^2}{R_r L_s^2}|\bar{\psi}_s^*|^2\right]\left[1 - e^{-\frac{t}{T_M}}\right]\omega_{sl}. \qquad (10)$$

From the above equation, the relationship between torque and slip angular frequency is quite clear. Dynamic torque response depends on the instantaneous slip angular frequency while the stator flux reference is kept constant. The torque can be controlled by using only one PI controller instead of hysteresis regulator (the classical DTC) for calculating the error

between reference and estimated torque. Then, the output of the PI torque controller will be used for calculating the stator flux angle. From (1) and (4), the estimated torque $\hat{T}_e$ of the motor in terms of the stator flux and the stator current in $\alpha\beta$ stationary reference frame can be written as

$$\hat{T}_e = \frac{3}{2}P\left(\tilde{\psi}_{\alpha s}i_{\beta s} - \tilde{\psi}_{\beta s}i_{\alpha s}\right) \qquad (11)$$

Finally, the estimated stator flux components are

$$\hat{\psi}_{\alpha s} = \int (v_{s\alpha} - i_{\alpha s}R_s)\,dt$$
$$\hat{\psi}_{\beta s} = \int (v_{\beta s} - i_{\beta s}R_s)\,dt. \qquad (12)$$

B. Design of the PI Torque Controller

As shown in Fig. 1, the reference torque T_e^* is obtained from the output of the PI speed controller. Then, the reference torque is compared with the estimated torque $\tilde{T}_e$ to generate an error signal. This signal is the input of the PI torque controller that computes the value of the instantaneous slip angular frequency ω_{sl}^* required to adjust the stator flux angle. The output of PI torque controller can be expressed as

$$\omega_{sl}^* = k_p\left[\Delta T_e + \frac{1}{T_i}\int \Delta T_e dt\right]. \qquad (13)$$

The input of the polar-to-rectangular transformation of direct stator flux control is the reference stator angular frequency ω_s^*, which is obtained by adding electrical rotor angular frequency ω_r with instantaneous slip angular frequency and can be expressed as

$$\omega_s^* = \omega_r + \omega_{sl}^* \qquad (14)$$

The block diagram of the torque control loop is illustrated in Fig. 3.
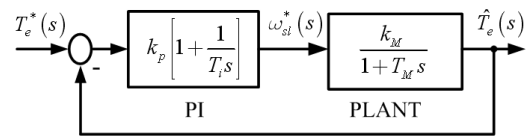
Fig.3: *Block diagram of the torque loop.*

By taking Laplace transform of (10) in order to determine $M(s)$ which is the relationship between the slip angular frequency $\omega_{sl}^*(s)$ and the actual torque $\hat{T}_e(s)$, the following equations can be achieved:

$$M(s) = \frac{\hat{T}_e(s)}{\omega_{sl}^*(s)} = \frac{k_M}{1 + T_M s}. \qquad (15)$$

where $k_M = \frac{3}{2}P\frac{L^2 m}{R_r L_s^2}|\bar{\psi}_s^*|^2$ is constant.

For PI controller design, the order of the system becomes one, which guarantees zero position steady-state error. With regard to pole placement, the output $\omega_{sl}^*(s)$ of the controller is obtained by Laplace transform of (13) and can be written as

$$\omega_{sl}^* = k_p\left[1 + \frac{1}{T_i s}\right]\left(T_e^*(s) - \hat{T}_e(s)\right) \qquad (16)$$

where k_p is the proportional gain; T_i is the integration time and let $\Delta T_e = \left(T_e^*(s) - \hat{T}_e(s)\right)$ is the error.

From Fig.3, by combining (15) and (16), the closed-loop transfer function $H(s)$ of the torque control system can be expressed as

$$H(s) = \frac{\hat{T}_e(s)}{T_e^*(s)} = \frac{\dfrac{k_M k_p}{T_M}s + \dfrac{k_M k_p}{T_i T_M}}{s^2 + \left(\dfrac{1}{T_M} + \dfrac{k_M k_P}{T_M}\right)s + \dfrac{k_M k_P}{T_i T_M}}. \quad (17)$$

For a unit-step command $(T_e^*(s) = 1/s)$, the actual torque is

$$\hat{T}_e(s) = \frac{\dfrac{k_M k_p}{T_M}s + \dfrac{k_M k_P}{T_i T_M}}{s^2 + \left(\dfrac{1}{T_M} + \dfrac{k_M k_P}{T_M}\right)s + \dfrac{k_M k_p}{T_i T_M}}\frac{1}{s}. \quad (18)$$

The characteristic polynomial is

$$s^2 + \left(\frac{1}{T_M} + \frac{k_M k_P}{T_M}\right)s + \frac{k_M k_P}{T_i T_M} = 0. \qquad (19)$$

The general form of the characteristic polynomial of a second-order system is given by,

$$s^2 + 2\zeta\omega_n s + \omega_n^2 = 0. \qquad (20)$$

where ω_n is the natural angular frequency for $\zeta \le 1$; ζ is the damping ratio.

Therefore, the natural angular frequency of the torque controller system is given by,

$$\omega_n = \sqrt{\frac{k_M k_P}{T_i T_M}} \qquad (21)$$

and the damping ratio is

$$\zeta = \left[\frac{1}{T_M} + \frac{k_M k_p}{T_M}\right]\sqrt{\frac{T_i T_M}{4 k_M k_p}}. \qquad (22)$$

The parameters of the PI controller might be calculated as

$$k_p = \frac{2\zeta\omega_n T_M - 1}{k_M} \qquad (23)$$

$$T_i = \frac{2\zeta\omega_n T_M - 1}{\omega_n T_M}. \qquad (24)$$

C. Direct Stator Flux Control

The main task of the direct stator flux control is decoupling the amplitude and the angle of the stator flux vector. The reference stator flux vector in polar form is given by $\bar{\psi}_s^* = |\bar{\psi}_s^*|\angle\rho_s^*$. The calculation of angle of the reference stator flux vector is obtained by integrating stator angular frequency ω_s^* as indicated in (14). As a consequence, the stator flux angle ρ_s^* is derived from

$$\rho_s^* = \int \omega_s^* dt. \qquad (25)$$

By polar-to-rectangular transformation of the stator flux vector, the reference stator flux components are expressed as follows:

$$\begin{aligned} \psi_{\alpha s}^* &= |\bar{\psi}_s^*|\cos\rho_s^* \\ \psi_{\beta s}^* &= |\bar{\psi}_s^*|\sin\rho_s^*. \end{aligned} \qquad (26)$$

Finally, from (1), the reference stator voltages $v_{\alpha s}^*$ and $v_{\beta s}^*$ in the $\alpha\beta$ frame are calculated based on forcing the stator flux error $(\Delta\psi_{\alpha s}(k)$ and $\Delta\psi_{\beta s}(k))$ to zero at the sampling period (k). The reference stator voltages $v_{\alpha s}^*(k)$ and $v_{\beta s}^*(k)$ are given by

$$v_{\alpha s}^*(k) = \left(\frac{\psi_{\alpha s}^*(k) - \hat{\psi}_{\alpha s}(k-1)}{\Delta T_s}\right) + R_s i_{\alpha s}(k-1)$$

$$v_{\beta s}^*(k) = \left(\frac{\psi_{\beta s}^*(k) - \hat{\psi}_{\beta s}(k-1)}{\Delta T_s}\right) + R_s i_{\beta s}(k-1). \quad (27)$$

where ΔT_s is the sampling interval, and k represents the actual discretized time.

From (27), the next reference stator voltages $v_{\alpha s}^*(k+1)$ and are applied to the induction motor using a SVM controlled inverter. In transient state, the reference stator voltage will be larger than the available inverter voltage when the torque error is quite large. In this case, the slip angular frequency ω_{sl}^* has to be limited to ensure the rated stator angular frequency $\omega_s = 2\pi f$. During under-modulation operation of SVM, the amplitude of the maximum available inverter voltage should be equal or less than $V_{dc}/\sqrt{3}$, where V_{dc} is the dc bus voltage of inverter.

D. Improved Stator Flux Estimator

The drawbacks of the estimation of the stator flux based on voltage model using open-loop integration

as shown in (12) are dc drift and saturation problems [21]-[23]. In this paper, improved stator flux estimator by integrating algorithm with an amplitude limiter in polar coordinates is used to overcome the problems associated with the pure integrator [24], [25]. The stator flux estimator is shown in Fig. 4
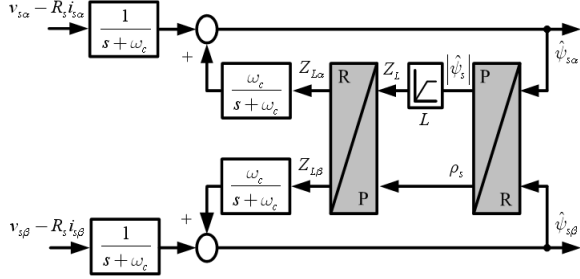
Fig.4: *Block diagram of the improved integrator algorithm with limited amplitude [24].*

In Fig. 4, the stator flux is transformed to polar coordinates and after limiting its amplitude it is transformed back to Cartesian coordinates. The limitation in Cartesian coordinates is performed as follows. The limited amplitude of the stator flux is defined as

$$
Z_L = \begin{cases} \sqrt{\hat{\psi}_{s\alpha}^2 + \hat{\psi}_{s\beta}^2} & \text{if } \sqrt{\hat{\psi}_{s\alpha}^2 + \hat{\psi}_{s\beta}^2} < L \\ L & \text{if } \sqrt{\hat{\psi}_{s\alpha}^2 + \hat{\psi}_{s\beta}^2} < L. \end{cases} \tag{28}
$$

where Z_L is the output of the limiter and L is the limit value. L should be equal to the stator flux reference. The limited components of the stator flux are then simply scaled with the ratio of the limited amplitude and unlimited amplitude

$$
Z_{L\alpha} = \frac{Z_L}{\sqrt{\hat{\psi}_{s\alpha}^2 + \hat{\psi}_{s\beta}^2}} + \hat{\psi}_{s\alpha}
$$
$$
Z_{L\beta} = \frac{Z_L}{\sqrt{\hat{\psi}_{s\alpha}^2 + \hat{\psi}_{s\beta}^2}} + \hat{\psi}_{s\beta}. \tag{29}
$$

where $Z_{L\alpha}$ and $Z_{L\beta}$ are the output limited values of the stator fluxes.
Finally, for a discrete-time implementation, the stator flux estimator can be written as

$$
\hat{\psi}_{s\alpha}(k+1) = \hat{\psi}_{s\alpha}(k) + (v_{s\alpha}(k) - R_s i_{s\alpha}(k))\Delta T_s (Z_{L\alpha} - \hat{\psi}_{s\alpha}(k))
$$
$$
\hat{\psi}_{s\beta}(k+1) = \hat{\psi}_{s\beta}(k) + (v_{s\beta}(k) - R_s i_{s\beta}(k))\Delta T_s (Z_{L\beta} - \hat{\psi}_{s\beta}(k))
$$
$$
\tag{30}
$$

where ω_c is the cutoff frequency of the low pass filter.

4. EXPERIMENTAL RESULTS

The experimental setup of the proposed control system is represented by the block diagram shown in

Fig. 5. It consists of a dSPACE DS1104 controller board with TMS320F240 slave processor, ADC interface board CP1104, and a four-pole induction motor with parameters listed in Table 1. A three phase VSI inverter is connected to supply 550V dc bus voltage, with the switching frequency and the dead time of 5 kHz and 4 μs, respectively. The DS1104 board is installed in Pentium IV 1.5 GHz PC for software development and results visualization. The control program is written in MATLAB/Simulink real time interface with sampling time of 100 μs.

Table 1: *Induction motor parameters.*

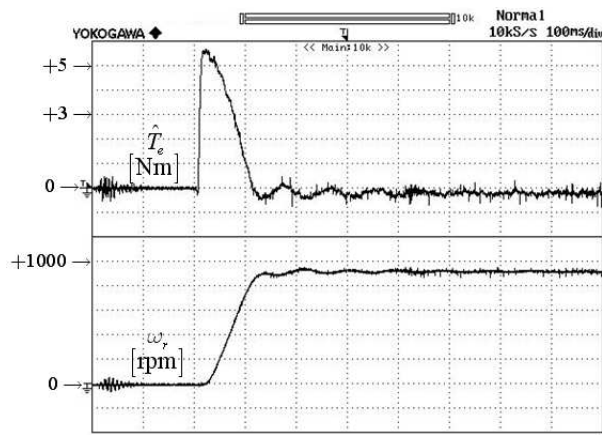| 3-phase | 0.37 kW | $R_s = 30\Omega$ |
50Hz	4-poles	$R_r = 31.49\Omega$
230/400V	1.8/1.05A	$L_s = 1.0942H$
$N_r = 1360$ rpm	$L_m = 1H$	$L_r = 1.0942H$
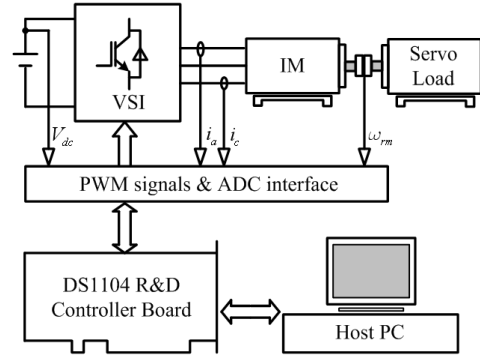
**Fig.5:** *Block diagram of experimental setup.*

The comparative starting transient performance is presented in Fig. 6. Much better performance for the DTC-AAS can be seen in Fig. 6(a). The estimated torque ripple is drastically reduced compared with Fig. 6(b) for the classical DTC. Also, fluctuation of measured rotor speed is illustrated due to the effect of the torque ripple.

Fig. 7 shows the torque transients step load change from no-load to full load and from full load to no-load. It can be seen that, small change in the stator flux amplitude, as shown in Fig. 7(a) is obtained for the proposed DTC-AAS. Again the ripple of torque and stator flux amplitude is high for the classical-DTC, as shown in Fig. 7(b).

Figs. 8 and 9 show the steady state responses from the classical DTC and the proposed DTC-AAS for no-load and full load operation at 900 rpm. In comparison with the classical DTC, the proposed DTC-AAS reduces the torque and stator flux ripple noticeably. It is noted that stator flux droop occurs for the classical DTC which is the problem as mentioned before. As shown in Fig 8, the stator current is nearly distorted by the sector changes as in the classical DTC and the stator current trajectory is circular.
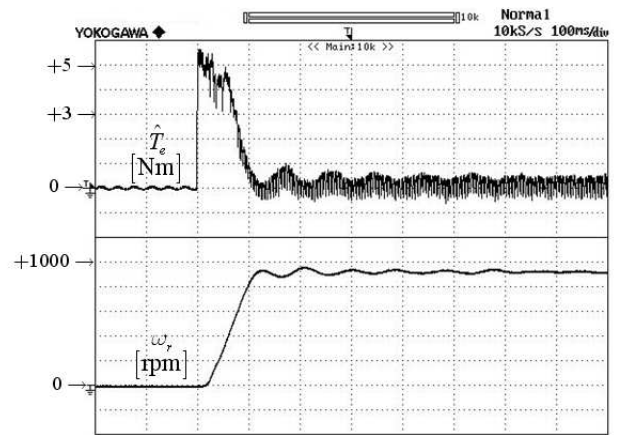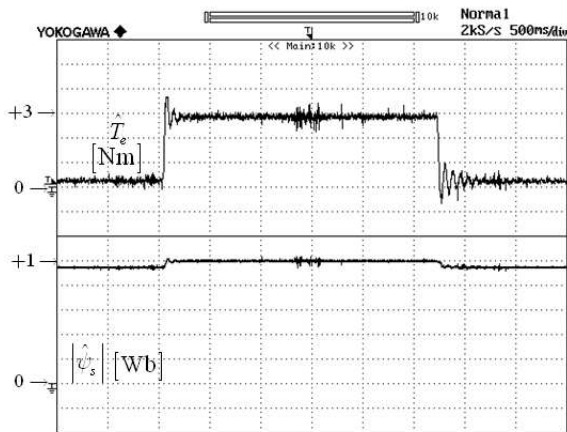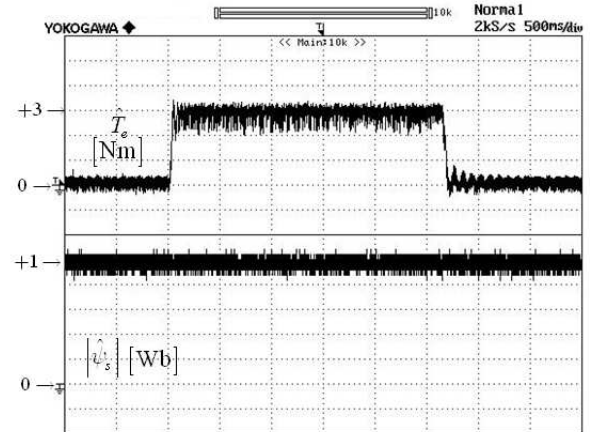
Fig.6: *Experimental results: Estimated torque and speed when the motor start-up to 900 rpm.*

Fig.7: *Experimental results: Estimated torque response and stator flux amplitude when step load torque change from no-load to full load (0 to 2.6 Nm).*

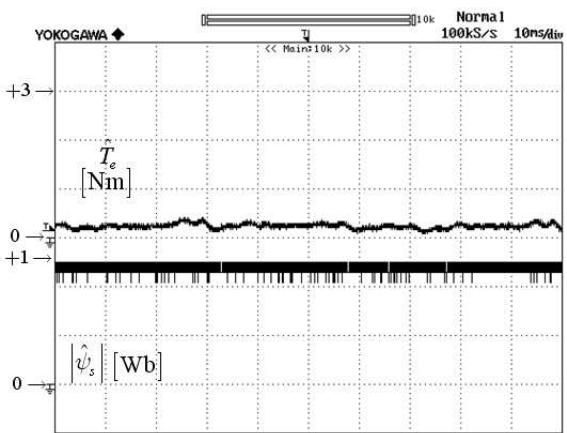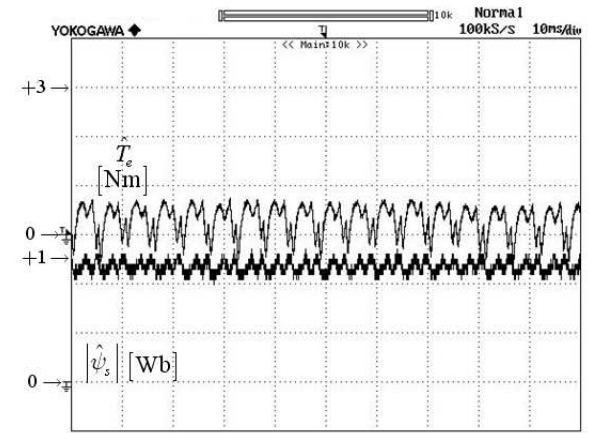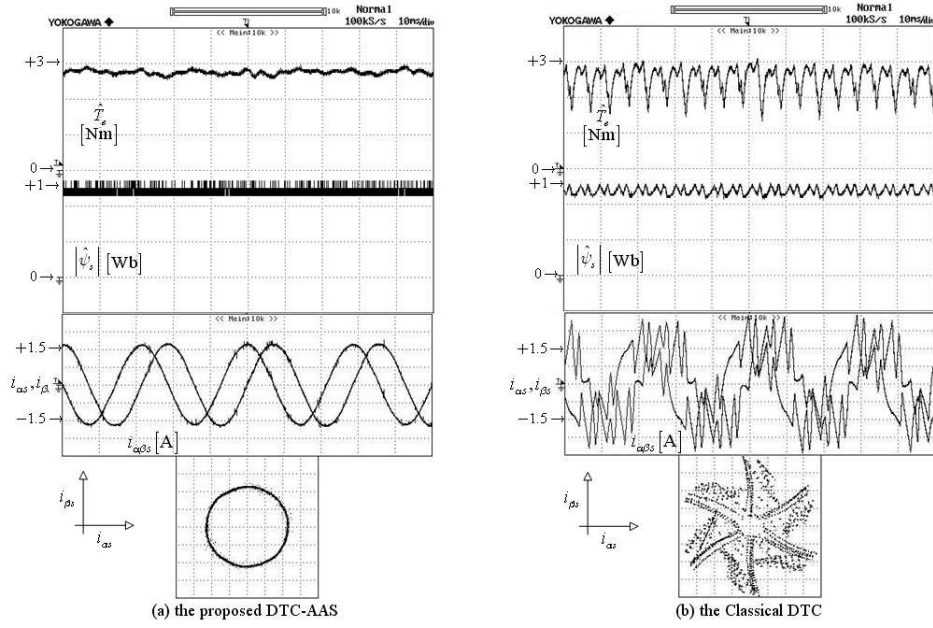**Fig.8:** *Experimental results: Estimated torque and stator flux amplitude in the no-load steady state with the speed of 900 rpm.*

(a) the proposed DTC-AAS

(b) the Classical DTC

Fig.9: *Experimental results: Estimated torque, stator flux amplitude, axis and stator current trajectory at 900 rpm under full load.*

(a) α -axis stator current and line to line stator voltage

(b) $\alpha\beta$ -axis and stator flux trajectory
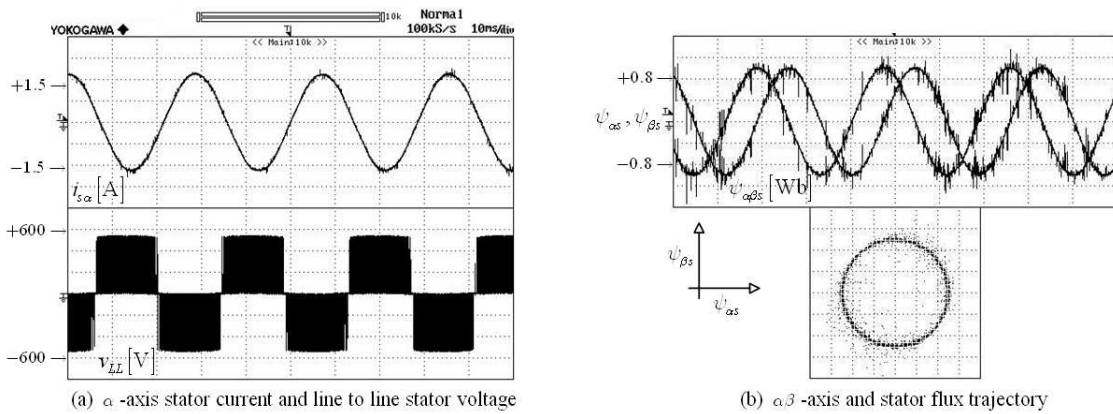
Fig.10: *Experimental results: Stator current (-axis), line to line stator voltage, axis and stator flux trajectory at 900 rpm under full load.*

(a) Speed and estimated torque

(b) Estimated stator flux and stator current α -axis
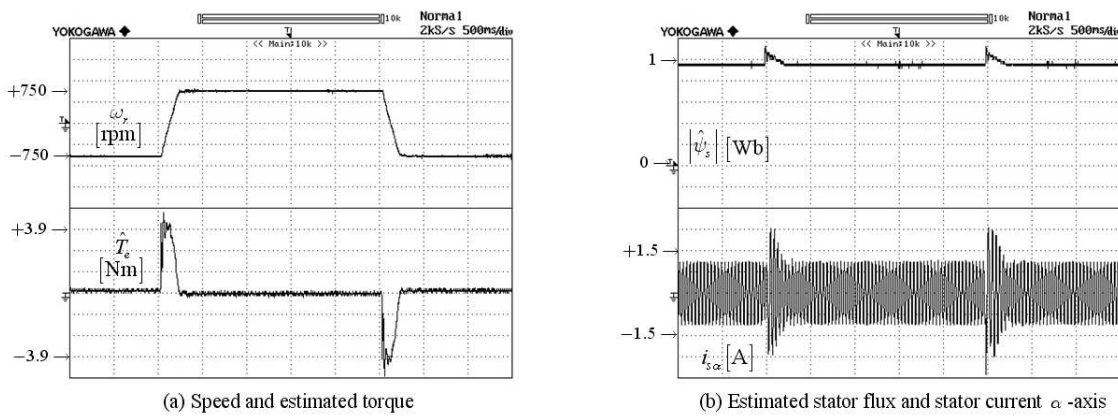
Fig.11: *Experimental results of the proposed DTC-AAS during speed reversal operation from -750 rpm to +750 rpm.*

(a) Stator flux angle, α -axis flux

(b) $\alpha\beta$ -axis and stator flux trajectory
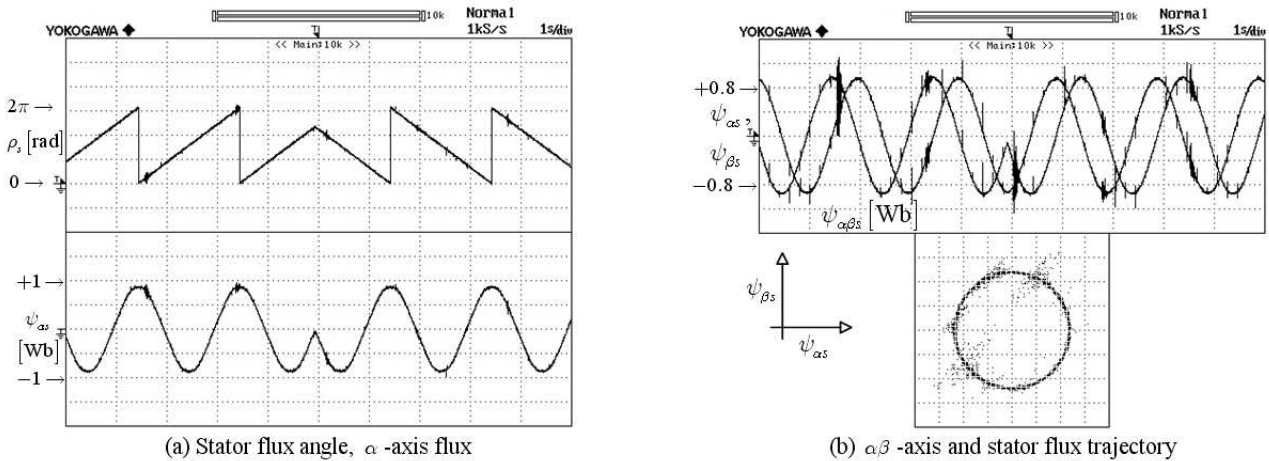
Fig.12: *Experimental results of the proposed DTC-AAS during speed reversal operation at 0.5Hz (±15rpm)*

As shown in Fig. 10, the stator flux waveform and its circular trajectory for the proposed DTC-AAS, line-to-line SVM motor voltage with 5 kHz switching frequency causes nearly sinusoidal stator current waveform.

Fig.11 shows the speed reversal from -750 rpm to +750 rpm and from +750 rpm to -750 rpm. Some small stator flux oscillations can be observed. The stator current increases during reversal operation. This performance confirms that decoupling operation between amplitude and angle of stator flux vector is able to deal with four quadrant operation.

Fig.12 shows the stator flux angle ρ_s and β axis stator flux waveform during speed reversal at low speed operation. It is quite clear that decoupling control between stator flux amplitude and stator flux angle occurs since the stator flux amplitude is constant while the stator flux angle changes rapidly during speed reversal operation. Also, the stator flux trajectory is still circular after a change in speed direction

5. CONCLUSIONS

This paper has presented the design and implementation of the SVM controlled inverter fed induction motor. The paper has proposed a decoupling between the amplitude and the angle of the reference stator flux for determining reference stator voltage vector in generating PWM output voltage for induction motors. The experimental results have shown that the proposed strategy has many advantages and features such as reduced torque ripple, reduced stator flux droop during sector change, smooth low speed operation, simple control with only one PI torque controller, decoupling operation between stator flux amplitude and stator flux angle, nearly sinusoidal stator current, and constant switching frequency. However, this technique requires accurate rotor speed which needs high resolution encoder.

References

[1] I. Takahashi and T. Noguchi, "A new quick response and high efficiency control strategy of an induction motor," *IEEE Trans. Ind. Appl.*, vol. IA-22, no. 5, pp. 820-827, 1986.

[2] G.S. Buja and M.P. Kazmierkowski, "Direct torque control of PWM inverter-fed AC motors - a survey," *IEEE Trans. Ind. Electron.*, vol. 51, pp. 744-757, 2004.

[3] M. P. Kazmierkowski and A. Kasprowicz, "Improved direct torque and flux vector control of PWM inverter-fed induction motor drive," *IEEE Trans. Ind. Electron.*, vol. 45, pp. 344-350, 1995.

[4] P.Vas, *Sensorless Vector and Direct Torque Control*. Oxford. U.K.:Oxford Univ. Prss, 1998.

[5] N. Mohan, *Advanced Electric Drives. Minneapolis*, MN: MNPERE, 2001.

[6] D. Casadai, G. Grandi, G. Serra, and A. Tani, "Effects of flux and torque hysteresis band amplitude in direct torque control of induction machines," in *Proc. IEEE IECON'94*, 1994, p. 299.

[7] C. G. Mei, S. K. Panda, J. X. Xu, and K. W. Lim, "Direct torque control of induction motors variable switching sectors," in *Proc. IEEE PEDS Conf.*, 1999, pp. 80-85.

[8] W.S.H. Wong and D. Holliday, "Minimization of flux droop in direct torque controlled induction motor drives," *IEE Proc. Electr. Power Appl.*, vol.151, no.6 pp. 694-703, 2004.

[9] T. G. Habetler, F. Profumo, M. Pastorelli, and L.M. Tolbert, "Direct torque control of induction motor using space vector modulation," *IEEE Trans. Ind.. Appl.*, vol. 28, no. 5, pp. 1045-1053, 1992.

[10] T.G. Habetler, F. Profumo, and M. Pastorelli, "Direct torque control of induction machines over a wide speed range," in *Proc. IEEE-IAS Conf.*, 1992, pp. 600-606.

[11] A. Tripathi, A. M. Khambadkone, and S. K.

Panda, "Space-vector based, constant frequency, direct torque control and dead beat stator flux control of AC machines," in *Proc. IEEE IECON'01*, 2001, p. 1219-1224.

[12] A. Mir, M. E. Elbuluk, and D. S. Zinger, "Fuzzy implementation of direct self control of induction motors," *IEEE Trans. Ind. Appl.*, vol. IA-22, no. 5, pp. 820-827, 1986.

[13] P. Z. Grabowski, M. P. Kazmierkowski, B. K. Bose, and F. Blaabjerg, "A simple direct-toque neuro-fuzzy control of PWM-inverter-fed induction motor drive," *IEEE Trans. Ind. Electron.*, vol. 30, pp. 729-735, 1994.

[14] C. Lascu, I. Boldea, and F. Blaabjerg, "A modified direct torque control for induction motor sensorless drive." *IEEE Trans. Ind. Appl.*, vol.36, no.1 pp. 122-130, 2000.

[15] C. Lascu and A. M. Trznaglowski, "A sensorless hybrid DTC drive for high-volume applications using the TMS320F243 DSP controller," in *Conf. Rec. IEEE-IAS. Annu. Meeting*, vol. 1, 2001, pp. 482-489.

[16] C. Lascu and A. M. Trznaglowski, "Combining the principles of sliding mode, direct torque control and space vector modulation in a high performance sensorless AC drive," in *Conf. Rec. IEEE-IAS. Annu. Meeting*, vol. 3, 2002, pp. 2073-2078.

[17] X. Xue, X. Xu, T.G. Habetler, and D. M. Divan, "A low cost stator flux oriented voltage source variable speed drive," in *Conf. Rec. IEEE-IAS. Annu. Meeting*, vol. 1, 1990, pp. 410-415.

[18] Y. S Lai and J. H. Chan, "A new approach to direct toque control of induction motor drive for constant inverter switching frequency and torque ripple reduction," *IEEE Trans. Energy Coners.*, vol.16, no. 3, pp. 220-227, 1992.

[19] L. Tang, L. Zhong, A. F. Rahman, and Y. Hu, "An investigation of a modified direct torque control strategy for flux and torque ripple reduction for induction machine drive system with fixed swiching frequency," in *Conf. Rec. IEEE-IAS Annu. Meeting*, vol. 2, 2002, pp. 837-844.

[20] J. Zhang and M. F. Rahman, "Analysis and design of a novel direct flux control scheme for induction machine," in *Conf. Rec. IEEE-IEMC'05*, 2005, pp. 426-430.

[21] B. K. Bose and N. R. Patel, "Quasifuzzy estimation of stator resistance of induction motor," *IEEE Trans. Power Electron.*, vol. 13, pp. 401-409, 1998.

[22] S. Mir, M. E. Elbuluk, and D. S. Zinger, "PI and fuzzy estimators for tuning the stator resistance in direct torque control of induction machines," *IEEE Trans. Power Electron.*, vol. 13, pp. 279-287, 1998.

[23] C. B. Jacabina, J. E. C. Filho, and A. M. N. Lima, "On-line estimation of the stator resistance of induction machines based on zero sequence model," *IEEE Trans. Power Electron.*, vol. 15, pp. 346-353, 2000.

[24] J. Hu and B. Wu, "New integration algorithms for estimating motor flux over a wide speed range," *IEEE Trans. Power Electron.*, vol. 13, pp. 969-977, 1998.

[25] Kuo-Kai Shoyu, Li-Jen Shang, Hwang-Zhi Chen, and Ko-wen Jwo, "Flux compensated direct torque control of induction motor drives for low speed operation," *IEEE Trans. Power Electron.*, vol. 19, pp. 1608-1613, 2004.

6. APPENDIX

By Laplace transform (9),

$$\hat{T}_e(s) = \mathcal{L}\left\{ k_M \left(1 - e^{-\frac{t}{T_M}}\right) \omega_{sl}\right\}$$

$$= k_M \omega_{sl} \mathcal{L}\left(1 - e^{-\frac{t}{T_M}}\right) = k_M \omega_{sl}\left(\frac{T_M s + 1 - T_M s}{s(1 + T_M s)}\right) A.1$$

$$= k_M \left(\frac{1}{(1 + T_M s)}\right)\frac{\omega_{sl}}{s}.$$

where

$$\omega_{sl}^*(s) = \frac{\omega_{sl}}{s} \qquad\qquad\qquad A.2$$

Thus, the transfer function of the torque loop $M(s)$ can be written as

$$M(s) = \frac{\hat{T}_e(s)}{\omega_{sl}^*(s)} = \frac{k_M}{1 + T_M s}. \qquad\qquad A.3$$

Yuttana Kumsuwan received the M.Eng. degree in electrical engineering from King Mongkut's Institute of Technology Ladkrabang (KMITL), Bangkok, Thailand, in 2001. and the Ph.D. degree in electrical engineering from the Chiang Mai University, Chiang Mai, Thailand, in 2007. From October 2007 to March 2008, he was a visiting Scholar with the Texas A&M University. Currently, he is a lecture in the Department of Electrical Engineering, Rajamangala University of Technology Lanna Tak Campus and Chiang Mai University, respectively. His research interests are in power electronics, electric drives and power quality.

Watcharin Srirattanawichaikul received the B.Eng. degree (First Class Honors) in electrical engineering from King Mongkut's Institute of Technology Ladkrabang (KMITL), Bangkok, Thailand, in 2006. He is currently studying toward his M.Eng. degree in Electrical Engineering at Chiang Mai University. His research interests are in power electronics, electric drives and control systems.

Suttichai Premrudeepreechacharn received the B.Eng. degree in electrical engineering from Chiang Mai University, Chiang Mai, Thailand, in 1988 and the M.S. and Ph.D. degree in electric power engineering from Rensselaer Polytechnic Institute, Troy, NY, in 1992 and 1997, respectively. Currently, he is an Associate Professor with the Department of Electrical Engineering, Chiang Mai University. His research interests include power electronics, electric drives, power quality, high-quality utility interfaces and artificial-intelligence-applied power system.